

Quantum metrology with one auxiliary particle in a correlated bath and its quantum simulation

Wan-Ting He (何宛亭),^{1,*} Huan-Yu Guang (光环宇) ^{1,*} Zi-Yun Li (李子贇),^{1,*} Ru-Qiong Deng (邓汝琼),^{2,1}
Na-Na Zhang (张娜娜),¹ Jie-Xing Zhao (赵洁杏),^{1,†} Fu-Guo Deng (邓富国) ¹ and Qing Ai (艾清) ^{1,‡}

¹*Department of Physics, Applied Optics Beijing Area Major Laboratory, Beijing Normal University, Beijing 100875, China*

²*School of Physics and Electronics, Hunan Normal University, Hunan 410006, China*



(Received 25 May 2021; revised 27 September 2021; accepted 29 November 2021; published 16 December 2021)

In realistic metrology, entangled probes are more sensitive to noise, especially for a correlated environment. The precision of parameter estimation with entangled probes is even lower than that of the unentangled ones in a correlated environment. In this paper we propose a measurement scheme with only one auxiliary qubit, which can selectively offset the impact of environmental noise under this situation. We analyze the estimation precision of our scheme and find out that it approaches the Heisenberg limit when prepared in a proper auxiliary state. We further discuss employing auxiliary states to improve the precision of measurement in other environment models such as a partially correlated environment. In order to verify our scheme, we apply a recently developed quantum algorithm to simulate the quantum dynamics of our proposal and show that it outperforms the other proposals with less resources.

DOI: [10.1103/PhysRevA.104.062429](https://doi.org/10.1103/PhysRevA.104.062429)

I. INTRODUCTION

Quantum metrology employs quantum entanglement and coherence to achieve an ultrahigh precision for the estimation of an unknown parameter [1,2]. It has become an indispensable element of satellite navigation, aerospace measurement and control, mobile phones, and computer chip processing. This opens a broad range of valuable applications of quantum mechanics, in addition to quantum information processing [3], photosynthetic exciton energy transfer [4,5], avian magnetoreception [4,6–8], and quantum metamaterial [9–12]. As a result of the central-limit theorem, the estimated precision of an unknown quantity critically depends on the number of resources available for the measurement. One of the primary goals of quantum metrology is to enhance the precision of resolution with limited resources. An enhanced resolution can be achieved if quantum entanglement is used to correlate the probes before making them interact with the system to be measured [13,14]. In quantum metrology, two-level quantum systems, i.e., qubits like electronic and nuclear spins, are widely considered as quantum probes [2]. Taking advantage of n entangled qubits with linear couplings, one can attain the Heisenberg limit (HL), which scales as n^{-1} , being the ultimate limit in precision set by quantum mechanics. And this result has been demonstrated experimentally [15,16]. On the contrary, when using unentangled qubits with linear couplings, one can only reach the standard quantum limit (SQL), which scales as $n^{-1/2}$. Obviously, the use of entanglement can significantly enhance the precision when n is large.

In realistic scenarios for experiments, quantum probes are inevitably affected by noise. The achievable precision decreases due to the decoherence. As known to all, the quantum dynamics of open quantum systems are usually classified into Markovian and non-Markovian [17–22]. When the system-bath couplings are relatively large, or the number of degrees of freedom in the environment is not sufficiently large, e.g., natural photosynthetic complexes and NV centers in diamond, the open quantum systems are subject to non-Markovian quantum dynamics [4,23]. Using entangled probes in a non-Markovian quantum dynamics allows for a higher measurement precision than that in a Markovian quantum dynamics, which scales as $n^{-3/4}$ [24,25]. A bound state outside the continuum can improve the precision of measurement [26,27]. On the other hand, when particles interact with a correlated environment, e.g., nuclear spins in a molecule, the decoherence rate per particle will increase linearly with the number of particles, i.e., superdecoherence [28,29]. In this regime, utilizing entangled probes will no longer outperform unentangled ones, no matter whether the open quantum dynamics is Markovian or non-Markovian.

In order to overcome decoherence in an uncorrelated bath, logical states are introduced to establish a decoherence-free subspace [30–32]. However, since N logical qubits require $n = 2N$ physical qubits, it doubles the number of valuable resources used per experiment. In order to effectively reduce the usage of resources, here we propose a measurement scheme with only one auxiliary qubit in a correlated bath. Using such a well-designed auxiliary particle in quantum metrology can selectively offset the impact of noise in a correlated environment. Comparing with previous proposals, we show that although we use less resources, we can still approach the HL when preparing proper auxiliary states.

On the other hand, although the theoretical scheme utilizing entanglement in a non-Markovian environment is

*These authors contributed equally to this work.

†zhaojiexing@mail.bnu.edu.cn

‡aiqing@bnu.edu.cn

appealing, it might be difficult to experimentally verify it since it critically requires the homogeneity of the qubits. For example, for NV centers in diamond, different spins manifest different Zeeman energies and decoherence rates in the same environment due to the inhomogeneous gyromagnetic ratios. Recently, based on the bath-engineering technique [33,34] and the gradient ascent pulse engineering (GRAPE) algorithm [35,36], we theoretically proposed and experimentally demonstrated that the open quantum dynamics with an arbitrary Hamiltonian and spectral density can be exactly and efficiently simulated [37,38]. Thus, based on this algorithm, we show how to verify that our scheme can make the estimation precision to achieve the HL in a quantum simulation experiment [39,40].

This paper is organized as follows: Our measurement scheme and its quantum dynamics for quantum metrology in a correlated bath are introduced in the next section. Specifically, we offer an example of magnetic-field sensing utilizing our measurement scheme. Then, in Sec. III we apply a recently developed quantum algorithm to simulate our measurement scheme with an auxiliary qubit and show that it can approach the HL. In the Appendix we provide a brief introduction for the GRAPE algorithm, which is an essential component in the quantum simulation approach [37,38].

II. MODEL AND DYNAMICS

A. Dynamics of n -qubit decoherence

The quantum dynamics of open system is described by the well-known spin-boson model [41,42]. Since the timescale of dephasing is generally much smaller than that of longitudinal relaxation, we consider the pure-dephasing dynamics for simplicity. The spin-boson Hamiltonian of n qubits coupled to a common bath can be written as [17,43–45]

$$H = \frac{1}{2} \hbar \omega_0 \sum_{i=1}^n \sigma_z^{(i)} + \sum_k \hbar \omega_k b_k^\dagger b_k + \sum_{i=1}^n \sigma_z^{(i)} \sum_k \hbar g_k^{(i)} (b_k^\dagger + b_k). \quad (1)$$

The system Hamiltonian is $H_S = \hbar \omega_0 \sum_{i=1}^n \sigma_z^{(i)}/2$, and the bath Hamiltonian is $H_B = \sum_k \hbar \omega_k b_k^\dagger b_k$, and the interaction Hamiltonian is $H_I = \sum_{i=1}^n \sigma_z^{(i)} \sum_k \hbar g_k^{(i)} (b_k^\dagger + b_k)$, where ω_0 is the energy separation between the ground and excited states, b_k^\dagger (b_k) is the creation (annihilation) bath operator, g_k is the coupling constant between the qubit and k th mode of bath, which is assumed to be real for simplicity.

The interaction Hamiltonian is the product of the system operators and the bath operators, i.e., $H_I = \sum_{i=1}^n s_i B_i$, with $s_i = \sigma_z^{(i)}$ and $B_i = \sum_k \hbar g_k^{(i)} (b_k^\dagger + b_k)$. We decompose the system operator s_i into several parts in the eigenspace $\{|\epsilon\rangle_i\}$ as $s_i = \sum_\omega s_i(\omega) |\epsilon\rangle_i \langle \epsilon'|$ with $s_i(\omega) = \sum_{\epsilon' - \epsilon = \omega} \langle \epsilon | s_i | \epsilon' \rangle_i$. The summation in $s_i(\omega)$ is extended over all energy eigenvalues ϵ and ϵ' of H_S with a fixed energy difference of ω [43,46]. Because $s_i = \sigma_z^{(i)}$, we have $s_i(\omega_0) = s_i(-\omega_0) = 0$ and $s_i(0) = \mp 1$ for $|0\rangle_i$ and $|1\rangle_i$, respectively. Introducing these eigenoperator decompositions, the Bloch-Redfield equation can be

rewritten as [42]

$$\dot{\rho} = \frac{i}{\hbar} [\rho, H_S] + \frac{1}{\hbar^2} \sum_{i,j=1}^n D_{ij}(0, t) (\sigma_z^{(j)} \rho \sigma_z^{(i)} - \frac{1}{2} \{ \sigma_z^{(i)} \sigma_z^{(j)}, \rho \}), \quad (2)$$

where $D_{ij}(\omega, t) = \int_0^t d\tau \exp(i\omega\tau) \langle \tilde{B}_i(\tau) \tilde{B}_j(0) \rangle$ are the spectral functions, which define both temporal and spatial correlations of the pure-dephasing noise environment [47]. $\tilde{B}_i(\tau) = \hbar g_k^{(i)} [b_k^\dagger \exp(i\omega_k\tau) + b_k \exp(-i\omega_k\tau)]$ are the operators of environment in the interaction picture, and $\langle \tilde{B}_i(\tau) \tilde{B}_j(0) \rangle$ are the correlation functions, i.e.,

$$\langle \tilde{B}_i(\tau) \tilde{B}_j(0) \rangle = \hbar^2 \sum_k g_k^{(i)} g_k^{(j)} [2\bar{n}(\omega_k, T) \cos \omega_k \tau + e^{-i\omega_k \tau}]. \quad (3)$$

Thus the spectral functions are explicitly given as

$$D_{ij}(\omega, t) = \hbar^2 \sum_k g_k^{(i)} g_k^{(j)} [2\bar{n}(\omega_k, T) \frac{\sin \omega_k t}{\omega_k} + \frac{1 - e^{-i\omega_k t}}{i\omega_k}]_{\omega_k = \omega}, \quad (4)$$

where $\bar{n}(\omega_k, T) = \langle b_k^\dagger b_k \rangle$ denotes the average occupation number of mode k at temperature T . The real part of $D_{ij}(0, t)$ causes dephasing, while its imaginary part corresponds to the Lamb shift [43]. Let $D_{ij}(0, t) = \frac{1}{2} C_{ij}(0, t) + i F_{ij}(0, t)$, and $H_{LS} = \sum_{i,j=1}^n F_{ij}(0, t) \sigma_z^{(i)} \sigma_z^{(j)}$ is the Lamb-shift Hamiltonian. Thus Eq. (2) is rewritten as

$$\dot{\rho} = \frac{i}{\hbar} [\rho, H_S + H_{LS}] + \frac{1}{2\hbar^2} \sum_{i,j=1}^n C_{ij}(0, t) \left(\sigma_z^{(j)} \rho \sigma_z^{(i)} - \frac{1}{2} \{ \sigma_z^{(i)} \sigma_z^{(j)}, \rho \} \right). \quad (5)$$

For $n = 1$, since the total Hamiltonian is $H = \hbar \omega_0 \sigma_z / 2 + \sum_k \hbar \omega_k b_k^\dagger b_k + \sigma_z \sum_k \hbar g_k (b_k^\dagger + b_k)$, Eq. (5) is simplified as

$$\dot{\rho} = \frac{i}{\hbar} \left[\rho, \frac{1}{2} \hbar \omega_0 \sigma_z \right] + \frac{1}{2\hbar^2} C(0, t) (\sigma_z \rho \sigma_z - \rho), \quad (6)$$

where the single-qubit dephasing rate is given by $\gamma(t) = C(0, t)/\hbar^2$.

However, the n -qubit dephasing rate varies with the environmental model. For simplicity, we assume that $g_k^{(i)} = g_k^{(j)} = g_k$. When n qubits are in an uncorrelated environment, e.g., the distance between the qubits are far beyond the correlation length of the environment [43], we can neglect all spatial correlations of the bath, i.e., $C_{ij}(0, t) = \hbar^2 \gamma(t) \delta_{ij}$. Hence the n -qubit dephasing rate is

$$\gamma_n(t) = \sum_{i,j=1}^n C_{i,j}(0, t) / \hbar^2 = n\gamma(t). \quad (7)$$

In contrast, when n qubits are in a correlated bath, i.e., the correlation length of the environment is much longer than the qubits' spatial separation, the n -qubit dephasing rate is n^2 times that of single qubit, i.e.,

$$\gamma_n(t) = n^2 \gamma(t), \quad (8)$$

resulting from $C_{ij}(0, t) = \hbar^2 \gamma(t)$ for all i and j . This phenomenon is called superdecoherence, mainly due to collective entanglement between qubits and the environment [48].

B. Quantum metrology under superdecoherence

In quantum metrology, using entangled probes can obtain an increase in precision when assuming a fully coherent evolution, while in realistic scenario, there is always decoherence caused by environmental noise. The optimal precision with entangled probes under decoherence was first analyzed in a Markovian environment [49] and further discussed in a non-Markovian environment [25]. The best resolution in the estimation was obtained with a given number of particles n and a total duration of experiment T , i.e., nT/t being the actual number of experiment for n uncorrelated probes, and T/t being the actual number of experiment for n entangled probes. Consider the Ramsey interferometer [25,49]. The entangled probes are prepared in an n -qubit GHZ state, $(|0\rangle^{\otimes n} + |1\rangle^{\otimes n})/\sqrt{2}$, and then evolve freely for a duration t . In the ideal case, we have $(|0\rangle^{\otimes n} + \exp(-in\phi t)|1\rangle^{\otimes n})/\sqrt{2}$, where ϕ is the parameter to be estimated. In realistic Ramsey interferometry experiments, $\hbar\phi$ is the energy splitting caused by an external field, e.g., the Zeeman effect and Stark effect. However, in the presence of dephasing noise, the final state becomes $\{|0\rangle\langle 0|^{\otimes n} + \exp[-in\phi t - \Gamma_n(t)]|0\rangle\langle 1|^{\otimes n} + \exp[in\phi t - \Gamma_n(t)]|1\rangle\langle 0|^{\otimes n} + |1\rangle\langle 1|^{\otimes n}\}/2$, with $\Gamma_n(t) = \int_0^t d\tau \gamma_n(\tau)$, and $\gamma_n(t)$ being the dephasing rate of n qubits. After a $\pi/2$ pulse, the probability of finding these probes in the initial state reads

$$P = \frac{1}{2} [1 + \cos(n\phi t) e^{-\Gamma_n(t)}]. \tag{9}$$

The uncertainty of the measurement can be calculated as

$$\delta\phi^2 = \frac{1}{(T/t)F(\phi)}, \tag{10}$$

where the Fisher information [46,50] is

$$F(\phi) \equiv \frac{1}{P(1-P)} \left(\frac{\partial P}{\partial \phi} \right)^2 = \frac{t^2 \sin^2(n\phi t) e^{-2\Gamma_n(t)}}{1 - \cos^2(n\phi t) e^{-2\Gamma_n(t)}}. \tag{11}$$

When the entangled probes are in an uncorrelated environment, we can obtain $\Gamma_n(t) = n \int_0^t d\tau \gamma(\tau) = n\Gamma(t)$, where $\gamma(t)$ and $\Gamma(t)$ are respectively the dephasing rate and decoherence factor for a single qubit. Thus the uncertainty is explicitly written as [25,49]

$$\delta\phi^2 = \frac{1 - \cos^2(n\phi t) e^{-2n\Gamma(t)}}{n^2 T t \sin^2(n\phi t) e^{-2n\Gamma(t)}}. \tag{12}$$

In order to attain the best precision, it is necessary to optimize this expression of uncertainty against the duration of each single measurement t . The best interrogation time satisfies $n\phi t_e = k\pi/2$ with odd k and $2nt \frac{d\Gamma(t)}{dt} |_{t=t_e} = 1$ [25], and thus yields

$$\delta\phi^2 |_e = \frac{1}{n^2 T t_e} e^{2n\Gamma(t_e)}, \tag{13}$$

where the subscript e indicates that the entangled probes are used.

TABLE I. The relative parameter resolution r varies with different dephasing dynamics.

	Uncorrelated environment	Correlated environment
Markovian	$r = 1$	$r = n^{-1/4}$
Non-Markovian	$r = n^{1/4}$	$r = 1$

As shown in the previous section, when the entangled probes are in a correlated environment, the decay rate is proportional to the square of the number of qubits, i.e., the superdecoherence [28,48,51,52]. As a result, the superdecoherence of the probes will modify the probability as

$$P = \frac{1}{2} [1 + \cos(n\phi t) e^{-n^2\Gamma(t)}]. \tag{14}$$

The uncertainty of parameter ϕ reads

$$\delta\phi^2 |_e = \frac{1 - \cos^2(n\phi t) e^{-2n^2\Gamma(t)}}{n^2 T t \sin^2(n\phi t) e^{-2n^2\Gamma(t)}}. \tag{15}$$

By minimizing $\delta\phi^2 |_e$, i.e., requiring that $n\phi t_e = k\pi/2$ with odd k and $2n^2 t \frac{d\Gamma(t)}{dt} |_{t=t_e} = 1$, we have

$$\delta\phi^2 |_e = \frac{1}{n^2 T t_e} e^{2n^2\Gamma(t_e)}. \tag{16}$$

When utilizing unentangled probes, the uncertainty of the parameter is $\delta\phi^2 |_u = \exp[2\Gamma(t_u)]/nTt_u$, and the best interrogation time is given by $\phi t_u = k\pi/2$ with odd k and $2t \frac{d\Gamma(t)}{dt} |_{t=t_u} = 1$ [25]. Following Ref. [25], we define

$$r = \frac{\delta\phi |_u}{\delta\phi |_e}, \tag{17}$$

where $|\delta\phi|_e$ and $|\delta\phi|_u$ are the standard deviation of the estimated parameter ϕ when using entangled and unentangled probes, respectively. Here r characterizes the improved precision of measurement for using entangled probes instead of unentangled ones. For entangled probes in an uncorrelated environment, we obtain $r^2 = n(t_e/t_u) \exp[2\Gamma(t_u) - 2n\Gamma(t_e)]$, while for entangled probes in a correlated environment, we have $r^2 = n(t_e/t_u) \exp[2\Gamma(t_u) - 2n^2\Gamma(t_e)]$. Obviously, r changes along with the dependence of function $\Gamma(t)$ on time [25], i.e., the dynamics of decoherence. For example, $\Gamma(t) \propto t$ corresponds to the Markovian dephasing dynamics. When $\Gamma(t)$ has a quadratic behavior, i.e., $\Gamma(t) \propto t^2$, it is the non-Markovian dephasing dynamics, which is actually the quantum Zeno dynamics [31,53–55]. Hereafter we just follow the terminology in Ref. [25]. In Table I we analyze the relative resolution of the parameter r in different situations, i.e., Markovian vs non-Markovian dynamics and correlated vs uncorrelated environments. We can learn from Table I that using entangled probes cannot improve the precision in the presence of superdecoherence because $r \leq 1$ for $n \geq 2$.

C. Quantum metrology using an auxiliary particle

As shown in the previous section, on account of superdecoherence, the best precision with entangled probes will no longer be superior to that with unentangled ones. Previous works [30,31] introduced logical states which are

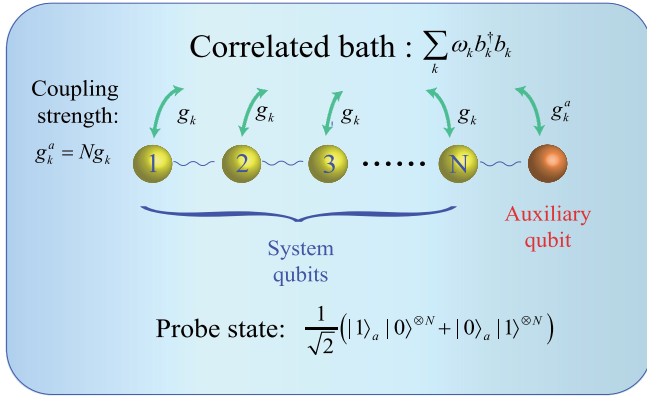


FIG. 1. Schematic for N qubits and one auxiliary qubit in a correlated bath. An $(N + 1)$ qubit entangled system, initially at $|\Psi(0)\rangle = (|1_a\rangle|0\rangle^{\otimes N} + |0_a\rangle|1\rangle^{\otimes N})/\sqrt{2}$, interacts with a correlated bath. The coupling constants between the qubits and the k th mode of the bath satisfy $g_k^a = Ng_k$.

decoherence-free to improve the precision at the cost of doubled resources used per experiment. In this section we present a measurement scheme with auxiliary states, only one auxiliary qubit being used per experiment. When we prepare a properly designed auxiliary qubit, the precision of parameter estimation can approach the HL.

As illustrated in Fig. 1, we initially prepare an $(N + 1)$ -qubit entangled state with N being the number of working qubits, i.e.,

$$|\Psi(0)\rangle = \frac{1}{\sqrt{2}}(|1_a\rangle|0\rangle^{\otimes N} + |0_a\rangle|1\rangle^{\otimes N}), \quad (18)$$

where the subscript a indicates the auxiliary qubit.

The total system is governed by the Hamiltonian $H = H_S + H_B + H_{\text{int}}$, H_S and H_B being the Hamiltonian of probe and bath, H_{int} being the interaction Hamiltonian:

$$H = \frac{1}{2}\hbar\Omega_0 \sum_{i=1}^N \sigma_z^{(i)} + \frac{1}{2}\hbar\omega_a \sigma_z^a + \sum_k \hbar\omega_k b_k^\dagger b_k + \sum_k \sum_{i=1}^N \hbar(g_k^{(i)} \sigma_z^{(i)} + g_k^a \sigma_z^a)(b_k^\dagger + b_k), \quad (19)$$

where ω_a is the frequency of the auxiliary qubit, we assume identical frequency Ω_0 for the N working qubits, $\sigma_z^{(i)}$ and σ_z^a are the Pauli operators of the working and auxiliary qubits, respectively, g_k (g_k^a) denotes the coupling constant between the working (auxiliary) qubit and the k th mode of the environment, b_k^\dagger is the creation operator of the harmonic oscillator with frequency ω_k .

According to Eq. (5), the quantum dynamics of the reduced density matrix of the total system including the working and auxiliary qubits is described by the quantum master equation

$$\dot{\rho} = \frac{i}{\hbar}[\rho, H_S + H_{\text{LS}}] + \frac{1}{2\hbar^2} \left[\sum_{i,j=1}^N C_{ij}(0, t) \left(\sigma_z^{(j)} \rho \sigma_z^{(i)} - \frac{1}{2} \{ \sigma_z^{(i)} \sigma_z^{(j)}, \rho \} \right) \right]$$

$$\begin{aligned} & + \sum_{i=1}^N C_{ia}(0, t) \left(\sigma_z^a \rho \sigma_z^{(i)} - \frac{1}{2} \{ \sigma_z^{(i)} \sigma_z^a, \rho \} \right) \\ & + \sum_{i=1}^N C_{ai}(0, t) \left(\sigma_z^{(i)} \rho \sigma_z^a - \frac{1}{2} \{ \sigma_z^a \sigma_z^{(i)}, \rho \} \right) \\ & + C_{aa}(0, t) (\sigma_z^a \rho \sigma_z^a - \rho) \end{aligned}, \quad (20)$$

where the time correlation functions are

$$C_{AB}(\omega, t) = 2\hbar^2 \sum_k g_k^A g_k^B [2\bar{n}(\omega_k, T) + 1] \frac{\sin \omega_k t}{\omega_k} \Big|_{\omega_k=\omega} \quad (21)$$

for $A, B = i, j, a$, with $\bar{n}(\omega_k, T)$ being the Bose-Einstein distribution at temperature T , $\{A, \rho\} = A\rho + \rho A$ is the anti-commutator,

$$\begin{aligned} H_{\text{LS}} = & \sum_{i,j=1}^N F_{ij}(0, t) \sigma_z^{(i)} \sigma_z^{(j)} + \sum_{i=1}^N F_{ia}(0, t) \sigma_z^{(i)} \sigma_z^a \\ & + \sum_{i=1}^N F_{ai}(0, t) \sigma_z^a \sigma_z^{(i)} + F_{aa}(0, t) \mathbb{I} \end{aligned} \quad (22)$$

is the Hamiltonian with the Lamb shift

$$F_{AB}(\omega, t) = \hbar \sum_k g_k^A g_k^B \frac{\cos \omega_k t - 1}{\omega_k} \Big|_{\omega_k=\omega} \quad (23)$$

for $A, B = i, j, a$, and \mathbb{I} is the identity operator.

1. Correlated environment

Suppose entangled probes are physically close, i.e., $g_k^{(j)} = g_k$ for $j = 1, 2, \dots, N$. They may suffer from superdecoherence with the time correlation function $C_{ij}(0, t) = \hbar^2 \gamma(t)$ for $i, j = 1, 2, \dots, N$. As illustrated in Fig. 1, in our measurement scheme, we prepare a proper auxiliary qubit whose coupling constant with the k th mode in the bath reads $g_k^a = Ng_k$. Thus we have $C_{ia}(0, t) = C_{ai}(0, t) = N\hbar^2 \gamma(t)$, and $C_{aa} = N^2 \hbar^2 \gamma(t)$. Equation (20) is rewritten as

$$\begin{aligned} \dot{\rho} = & \frac{i}{\hbar}[\rho, H_S + H_{\text{LS}}] \\ & + \frac{1}{2} \left[\sum_{i,j=1}^N \gamma(t) \left(\sigma_z^{(j)} \rho \sigma_z^{(i)} - \frac{1}{2} \{ \sigma_z^{(i)} \sigma_z^{(j)}, \rho \} \right) \right. \\ & + N \sum_{i=1}^N \gamma(t) \left(\sigma_z^a \rho \sigma_z^{(i)} - \frac{1}{2} \{ \sigma_z^{(i)} \sigma_z^a, \rho \} \right) \\ & + N \sum_{i=1}^N \gamma(t) \left(\sigma_z^{(i)} \rho \sigma_z^a - \frac{1}{2} \{ \sigma_z^a \sigma_z^{(i)}, \rho \} \right) \\ & \left. + N^2 \gamma(t) (\sigma_z^a \rho \sigma_z^a - \rho) \right]. \end{aligned} \quad (24)$$

For simplicity, we denote $|1\rangle \equiv |0_a\rangle|1\rangle^{\otimes N}$ and $|2\rangle \equiv |1_a\rangle|0\rangle^{\otimes N}$. The diagonal terms of the density matrix are constant in time, while the off-diagonal term is given by

$$\rho_{12}(t) = e^{i(N\Omega_0 - \omega_a)t} \rho_{12}(0). \quad (25)$$

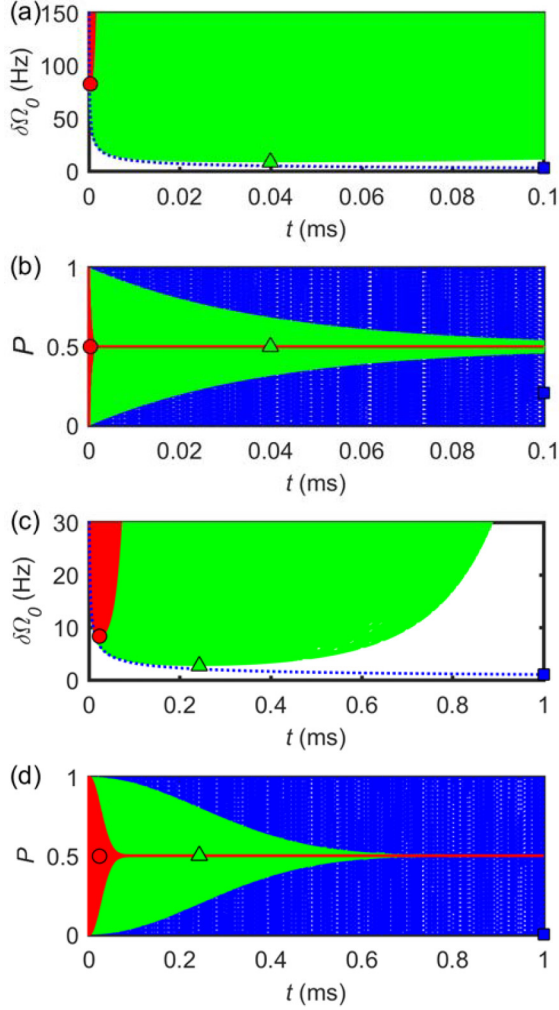


FIG. 2. The uncertainty of the measurement $\delta\Omega_0$ for (a) a Markovian dephasing dynamics with $\Gamma(t) = \alpha t$, (c) a non-Markovian dynamics with $\Gamma(t) = \beta t^2$. Equation (26) for (b) a Markovian dephasing dynamics, (d) a non-Markovian dynamics. The dashed green (light gray) line indicates the uncorrelated decoherence. The solid red (dark gray) line indicates the superdecoherence in correlated environment. And the dotted blue (black) line indicates our scheme. The green triangle, red circle, and blue square show the best interrogation time for uncorrelated decoherence, superdecoherence, and our scheme, respectively. We use the following parameters: $N = 100$, $\Omega_0 = 2\pi \times 411.5$ THz, $\alpha = 125$ s $^{-1}$, $\beta = 4.2473 \times 10^4$ s $^{-2}$, $T = 0.1$ s [52,56]. The rapid oscillations are overcrowded due to $\Omega_0 \gg \alpha$.

As in the conventional quantum metrology scheme, after a free evolution for a time interval t and a $\pi/2$ pulse, the probability of finding the probes in the initial state reads

$$P = \frac{1}{2}[1 + \cos(N\Omega_0 - \omega_a)t]. \quad (26)$$

We investigate Eq. (26) for different decoherence dynamics in Fig. 2. According to Eq. (16), the entangled probes have a higher precision when experiencing a longer evolution time t_e . Since the best interrogation time for the correlated bath is much shorter than that for the uncorrelated bath, the precision for the former is much worse. However, in our scheme, the

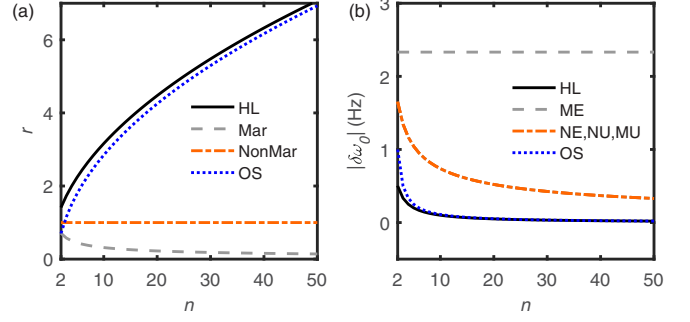


FIG. 3. (a) The relative ratio $r = |\delta\omega_0|_u/|\delta\omega_0|_e$ and (b) the standard deviation $|\delta\omega_0|$ of the measured frequency of the entangled and unentangled probes when suffering from superdecoherence. The black solid line represents the noise-free HL, and the blue dotted line shows our scheme with only one auxiliary qubit. When there are no auxiliary qubits, ME (MU) and NE (NU) correspond to the entangled (unentangled) probes in the Markovian and non-Markovian environment, respectively.

HL can be recovered because the effects of the noises on the working qubits have been effectively canceled due to the auxiliary qubit. We further compare the case in non-Markovian dynamics with the one in Markovian dynamics. The best interrogation times are longer for the former, which is consistent with the prediction in Ref. [25].

According to Eq. (16), the best resolution in the estimation satisfies $(N\Omega_0 - \omega_a)t_e = k\pi/2$ with odd k . The uncertainty in our scheme reads

$$\delta\omega_0^2|_e = \frac{1}{N^2 T t_e} = \frac{1}{(n-1)^2 T t_e} \propto \frac{1}{(n-1)^2}, \quad (27)$$

where $n = N + 1$. N is smaller than n due to the auxiliary qubit.

For unentangled probes, each probe needs a properly designed auxiliary qubit to cancel the effects of the noises on it. The uncertainty of the measurement is

$$\delta\omega_0^2|_u = \frac{1}{N' T t_u} = \frac{2}{n T t_u} \propto \frac{1}{n}, \quad (28)$$

where the best interrogation time t_u is given by $(\Omega_0 - \omega_a)t_u = k\pi/2$ with odd k . In this case, $n = 2N'$ and thus only half of the qubits play the role as the working qubits.

Based on the quantum dynamics shown in Fig. 2, we compare the uncertainty of measurement with and without auxiliary qubits in the presence of superdecoherence. In Fig. 3 we consider two cases, i.e., the noise is fully Markovian with $\Gamma(t) \propto t$ or non-Markovian dynamics with $\Gamma(t) \propto t^2$. In Fig. 3(b), the standard deviation of the measured frequency $|\delta\omega_0|_u$ and $|\delta\omega_0|_e$ are set to be equal for $n = 1$. And the lines of unentangled probes in the Markovian bath, and entangled and unentangled probes in the non-Markovian bath, are overlapped. When the noise is of non-Markovian dynamics, r remains unity for different n 's, as $|\delta\omega_0|_u = |\delta\omega_0|_e \propto n^{-1/2}$. It implies that the precision of measurement cannot be improved by using the entangled probes. When the noise is Markovian, $|\delta\omega_0|_e$ is a constant for different n 's, while $|\delta\omega_0|_u \propto n^{-1/2}$. r approaches zero as n increases, which suggests that using the entangled probes may even worsen the precision in the

presence of superdecoherence. However, if one auxiliary qubit is employed to cancel the effects of noise, the precision in our scheme can approach the HL.

In the above consideration, we only investigate the quantum dynamics for the GHZ state. We can also choose other forms of the initial state $(|1_m\rangle + |2_m\rangle)/\sqrt{2}$ to start with, where $|1_m\rangle = |0_a\rangle|0\rangle^{\otimes m}|1\rangle^{\otimes(N-m)}$, $|2_m\rangle = |1_a\rangle|1\rangle^{\otimes m}|0\rangle^{\otimes(N-m)}$, the integer $m \in [0, N]$. Assuming that $g_k^a/g_k = K$, the reduced density matrix of the total system is described by the quantum master equation, i.e.,

$$\dot{\rho}_{12}^m = i[(N-2m)\Omega_0 - \omega_a]\rho_{12}^m - \gamma(t)(N-K-2m)^2\rho_{12}^m, \quad (29)$$

where $\rho_{12}^m = \langle 1_m|\rho|2_m\rangle$. Let $K = N - 2m$ to offset the impact of correlated noise. The probability of finding the probes in the initial state reads

$$P = \frac{1}{2}\{1 + \cos[(N-2m)\Omega_0 - \omega_a]t\}. \quad (30)$$

According to Eq. (8), the best resolution in the estimation satisfies $[(N-2m)\Omega_0 - \omega_a]t_e = k\pi/2$ with odd k . The uncertainty thus reads

$$\delta\omega_0^2|_e = \frac{1}{(N-2m)^2 T t_e} \propto \frac{1}{(n-2m-1)^2}. \quad (31)$$

According to Eqs. (28) and (31), the relative ratio $r \propto (n-2m-1)/\sqrt{n}$. It can be greater than 1 as long as $n - \sqrt{n} > 2m + 1$. In other words, using initial states other than the GHZ state, the precision can be improved over the unentangled state. Furthermore, since r reaches its maximum when $m = 0$, it implies that the initial state used in our scheme is optimal.

2. Uncorrelated environment

When all probes are placed in an uncorrelated environment, e.g., they are spatially separated, the correlation function becomes $C_{ij}(0) = \hbar^2\gamma(t)\delta_{ij}$, and the quantum master equation (20) is simplified as

$$\dot{\rho} = \frac{i}{\hbar}[\rho, H_S + H_{LS}] + \frac{1}{2}\left[\sum_i \gamma(t)(\sigma_z^{(i)}\rho\sigma_z^{(i)} - \rho) + \frac{C_{aa}(0, t)}{\hbar^2}(\sigma_z^a\rho\sigma_z^a - \rho)\right]. \quad (32)$$

Let $K = g_k^a/g_k$. Consequently, we have $C_{aa}(0, t) = K^2\hbar^2\gamma(t)$. The off-diagonal element of the density matrix follows the evolution

$$\rho_{12}(t) = \rho_{12}(0)e^{i(N\Omega_0 - \omega_a)t} e^{-(N+K^2)\int\gamma(t')dt'}. \quad (33)$$

Since $N + K^2 > N$, using auxiliary qubits cannot reduce but increases the dephasing of probes. As a consequence, our measurement scheme cannot improve the precision of measurement in the case of uncorrelated environments.

3. Partially correlated environment

In this section we consider a partially correlated environment. Assume that all qubits, including N working qubits and one auxiliary qubit, are spatially arranged in a linear array, as

shown in Fig. 1. Following Ref. [43], the real-valued homogeneous correlation functions $C_{ij}(0, t)$, $C_{ia}(0, t)$, and $C_{ai}(0, t)$ read, respectively,

$$C_{ij}(0, t) = \hbar^2 e^{-x|i-j|}\gamma(t), \quad (34)$$

$$C_{ia}(0, t) = C_{ai}(0, t) = \hbar^2 K e^{-x(N+1-i)}\gamma(t), \quad (35)$$

where $x = d/\xi$, with d being the spatial distance between two adjacent qubits and ξ the environmental correlation length [43]. For an uncorrelated bath, we have $\xi = 0$ and $C_{ij} = \delta_{ij}\hbar^2\gamma(t)$, while $\xi = \infty$ and $C_{ij} = \hbar^2\gamma(t)$ for any i and j in a fully correlated bath. Generally, a finite but nonvanishing ξ corresponds to a partially correlated bath. The off-diagonal term of the density matrix is given by

$$\rho_{12}(t) = \rho_{12}(0)e^{i(N\Omega_0 - \omega_a)t} e^{-A(N, x)\int\gamma(t')dt'}, \quad (36)$$

where the factor

$$A(N, x) = (K-a)^2 + b - a^2, \quad (37)$$

$$a = \sum_{i=1}^n \exp[-x(N+1-i)], \quad (38)$$

$$b = \sum_{i,j=1}^n \exp(-x|i-j|). \quad (39)$$

Here $A(N, a)\gamma(t)$ represents the total dephasing rate of the working and auxiliary qubits. In order to improve the precision of measurement, we can always choose a proper K to minimize the factor $A(N, x)$. After some algebra we have

$$r = \begin{cases} \left[\frac{A(1, x)}{A(N, x)}\right]^{1/4} \left[\frac{2(n-1)^2}{n}\right]^{1/2}, & x > 0, \\ \left[\frac{2(n-1)^2}{n}\right]^{1/2}, & x = 0. \end{cases} \quad (40)$$

Therefore, employing auxiliary qubits can also improve the precision of a measurement for the entangled probes in a partially correlated environment.

D. Example for magnetic-field sensing

As known to all, the direction and magnitude of the geomagnetic field are closely related to the position on the earth. Thus various schemes have been put forward to measure the magnetic field in order to utilize geomagnetics for navigation, e.g., the radical pair mechanism [4] for avian navigation and the decoherence behaviors of the NV center in diamond [57–61]. In this section, as an example we show how to utilize our measurement scheme with one auxiliary qubit in magnetic-field sensing. The initial state of the entangled probes with N working qubits and one auxiliary qubit is prepared in $|\Psi(0)\rangle = (|1\rangle_a|0\rangle^{\otimes N} + |0\rangle_a|1\rangle^{\otimes N})/\sqrt{2}$, where $|0\rangle$ and $|1\rangle$ refer to the parallel and antiparallel spin states with respect to the magnetic field, respectively. Then, let the probe be exposed to a magnetic field B . After a time interval t , it evolves into

$$\rho(t) = \frac{1}{2} [|1\rangle_a\langle 1|_a(|0\rangle\langle 0|)^{\otimes N} + |0\rangle_a\langle 0|_a(|1\rangle\langle 1|)^{\otimes N} + e^{i(N\gamma_0 B - \gamma_a B)t} e^{-\Gamma(t)} |1\rangle_a\langle 0|_a(|0\rangle\langle 1|)^{\otimes N} + e^{-i(N\gamma_0 B - \gamma_a B)t} e^{-\Gamma(t)} |0\rangle_a\langle 1|_a(|1\rangle\langle 0|)^{\otimes N}], \quad (41)$$

where γ_0 (γ_a) is the gyromagnetic ratio of the working (auxiliary) qubit. By choosing an appropriate auxiliary qubit which satisfies $g_k^a = Ng_k$, we have $\Gamma(t) = 0$. The reduced density matrix of the working qubits at time t is given by

$$\begin{aligned} \rho(t) = & \frac{1}{2} [|1\rangle_a \langle 1|_a (|0\rangle \langle 0|)^{\otimes N} + |0\rangle_a \langle 0|_a (|1\rangle \langle 1|)^{\otimes N} \\ & + e^{i(N\gamma_0 B - \gamma_a B)t} |1\rangle_a \langle 0|_a (|0\rangle \langle 1|)^{\otimes N} \\ & + e^{-i(N\gamma_0 B - \gamma_a B)t} |0\rangle_a \langle 1|_a (|1\rangle \langle 0|)^{\otimes N}]. \end{aligned} \quad (42)$$

After a $\pi/2$ pulse, the probability of finding the probes in their initial state reads $P = [1 + \cos(N\gamma_0 B t - \gamma_a B t)]/2$. Here the Fisher information is given by

$$F(B) = \frac{(N\gamma_0 - \gamma_a)^2 t^2 \sin^2(N\gamma_0 B t - \gamma_a B t)}{1 - \cos^2(N\gamma_0 B t - \gamma_a B t)}. \quad (43)$$

Since the best interrogation time for the entangled probes is determined by $(N\gamma_0 B - \gamma_a B)t_e = k\pi/2$ with odd k , we calculate the uncertainty in the estimated value of B as

$$\delta B^2|_e = \frac{1}{(N\gamma_0 - \gamma_a)^2 T t}. \quad (44)$$

When N is large enough, the precision of measurement will approach the HL.

III. QUANTUM SIMULATION OF QUANTUM METROLOGY

In the NMR platform, we can use bath-engineering techniques and the GRAPE algorithm to simulate the quantum dynamics under superdecoherence. By this quantum simulation we can further prove that our measurement scheme with one auxiliary qubit can approach the HL, even in the case of superdecoherence. Utilizing the bath-engineering technique, we apply a time-dependent magnetic field to the total system, including the working and auxiliary qubits. The total system is governed by the Hamiltonian [37,38]

$$H = \frac{1}{2} \hbar \Omega_0 \sum_{i=1}^N \sigma_z^{(i)} + \frac{1}{2} \hbar \omega_a \sigma_z^a + \beta_1(t) \sum_{i=1}^N \sigma_z^{(i)} + \beta_2(t) \sigma_z^a, \quad (45)$$

with

$$\beta_1(t) = b_1 \sum_{j=1}^J \omega_j F(j) \cos(\omega_j t + \psi_{1j}), \quad (46)$$

$$\beta_2(t) = b_2 \sum_{j=1}^J \omega_j F(j) \cos(\omega_j t + \psi_{2j}), \quad (47)$$

where b_1 and b_2 are the noise amplitudes perceived by the working and auxiliary qubits, respectively. ω_0 ($\omega_j = J\omega_0$) is the base (cutoff) frequency with $\omega_j = j\omega_0$. $F(j)$ is the function which determines the type of noise, and ψ_{ij} ($i = 1, 2$) is a random number. All the parameters above can be manipulated manually. Here we apply identical time-dependent magnetic fields to all of the working qubits to simulate the superdecoherence. We further assume $b_2 = nb_1$ and $\psi_{1j} = \psi_{2j}$ to cancel the effects of the noise by the auxiliary qubit.

We divide the Hamiltonian (45) into two parts, i.e., the control Hamiltonian $H_c = \hbar(\Omega_0 \sum_{i=1}^N \sigma_z^{(i)} + \omega_a \sigma_z^a)/2$ and the

noise Hamiltonian $H_0(t) = \beta_1(t) \sum_{i=1}^N \sigma_z^{(i)} + \beta_2(t) \sigma_z^a$. In the Schrödinger picture, the propagator of this dynamics is given by

$$U(t) = U_c(t) \tilde{U}(t), \quad (48)$$

$$U_c(t) = e^{-\frac{i}{\hbar} (\Omega_0 t \sum_i \sigma_z^{(i)} + \omega_a t \sigma_z^a)}, \quad (49)$$

$$\tilde{U}(t) = e^{-\frac{i}{\hbar} \int_0^t d\tau \beta_1(\tau) \sum_i \sigma_z^{(i)}} e^{-\frac{i}{\hbar} \int_0^t d\tau \beta_2(\tau) \sigma_z^a}. \quad (50)$$

The initial state of the total system is $|\Psi(0)\rangle = [|1\rangle_a |0\rangle^{\otimes N} + |0\rangle_a |1\rangle^{\otimes N}] / \sqrt{2}$. Let it evolve for a time interval t under the Hamiltonian (45). Thus we have

$$\begin{aligned} |\psi(t)\rangle &= U(t) |\psi(0)\rangle \\ &= \frac{1}{\sqrt{2}} (e^{-i\varphi(t)} |1\rangle_a |0\rangle^{\otimes N} + e^{i\varphi(t)} |0\rangle_a |1\rangle^{\otimes N}), \end{aligned} \quad (51)$$

with the random phase accumulated in the simulation,

$$\varphi(t) = \varphi_A(t) + \varphi_B(t), \quad (52)$$

$$\varphi_A(t) = \frac{1}{2} (N\Omega_0 - \omega_a)t, \quad (53)$$

$$\varphi_B(t) = \frac{1}{\hbar} \left[N \int_0^t d\tau \beta_1(\tau) - \int_0^t d\tau \beta_2(\tau) \right]. \quad (54)$$

In order to mimic the effect of decoherence, we prepare a large number of ensembles which evolve under different Hamiltonians characterized by a set of the random numbers $\{\psi_{1j}, \psi_{2j} | j = 1, \dots, J\}$. Finally, the probability of finding the probes in the initial state is over the ensemble as

$$P_0(t) = \frac{1}{2} [1 + \cos 2\varphi_A \langle \cos 2\varphi_B \rangle - \sin 2\varphi_A \langle \sin 2\varphi_B \rangle]. \quad (55)$$

If we further assume a Gaussian noise, then we have $\langle \varphi_B^{2m-1}(t) \rangle = 0$ for any positive integer m [37], thus yielding

$$P_0(t) = \frac{1}{2} [1 + \cos 2\varphi_A(t) e^{-2\chi(t)}], \quad (56)$$

where

$$\chi(t) = \langle \varphi_B^2(t) \rangle = \frac{4}{2\pi \hbar^2} \int_{-\infty}^{+\infty} \frac{d\omega}{\omega^2} S(\omega) \sin^2 \frac{\omega t}{2},$$

$$S(\omega) = N^2 S_{11}(\omega) - N S_{12}(\omega) - N S_{21}(\omega) + S_{22}(\omega).$$

Here $S_{ij}(\omega) = \int_{-\infty}^{+\infty} dt \langle \beta_i(0) \beta_j(t) \rangle \exp(i\omega t)$ ($i, j = 1, 2$) is the Fourier transform of the two-time correlation function $\langle \beta_i(t_1) \beta_j(t_2) \rangle$, which depends on the time interval $t_2 - t_1$. And $S(\omega)$ is the total power spectral density of the noise, which describes the energy distribution of the stochastic signal in the frequency domain [37].

We utilize the relation that $b_2 = Nb_1$ and $\psi_{1j} = \psi_{2j}$ to obtain the two-time correlation functions as

$$\langle \beta_1(t + \tau) \beta_1(t) \rangle = \frac{b_1^2 \omega_0^2}{2} \sum_{j=1}^J j^2 F(j)^2 \cos(\omega_j \tau),$$

$$\begin{aligned} \langle \beta_1(t + \tau) \beta_2(t) \rangle &= \langle \beta_2(t + \tau) \beta_1(t) \rangle \\ &= \frac{N b_1^2 \omega_0^2}{4} \sum_{j=1}^J j^2 F(j)^2 \cos(\omega_j \tau), \end{aligned}$$

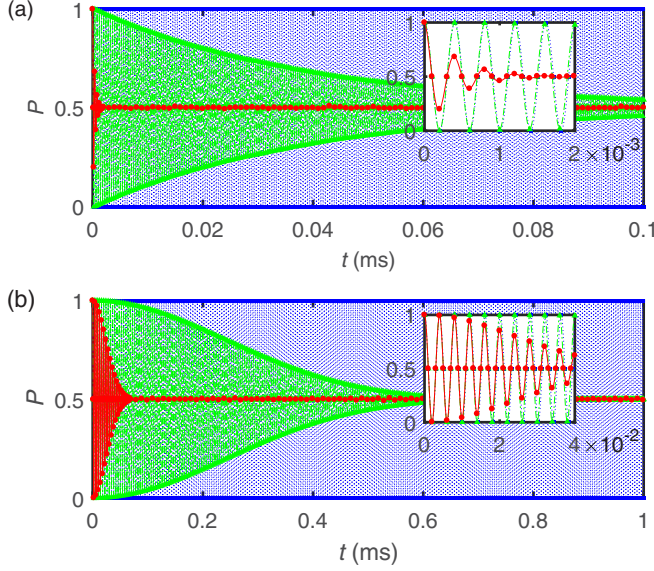


FIG. 4. Quantum simulation of population dynamics for (a) Markovian noise and (b) non-Markovian noise. The dashed green (light gray) line, the solid red (dark gray) line, and the dotted blue (black) line are the same as Fig. 2, while the green triangles, the red circle, and the blue squares are obtained by the quantum simulation approach [37,38] for the uncorrelated decoherence, the superdecoherence, and our scheme, respectively. The insets enlarge the short-time regime.

$$\langle \beta_2(t + \tau) \beta_2(t) \rangle = \frac{N^2 b_1^2 \omega_0^2}{2} \sum_{j=1}^J j^2 F(j)^2 \cos(\omega_j \tau).$$

Thus the power spectral densities are respectively given by

$$\begin{aligned} S_{11}(\omega) &= \frac{\pi b_1^2 \omega_0^2}{2} \sum_{j=1}^J j^2 F(j)^2 [\delta(\omega - \omega_j) + \delta(\omega + \omega_j)], \\ S_{12}(\omega) &= S_{21}(\omega) \\ &= \frac{N \pi b_1^2 \omega_0^2}{2} \sum_{j=1}^J j^2 F(j)^2 [\delta(\omega - \omega_j) + \delta(\omega + \omega_j)], \\ S_{22}(\omega) &= \frac{N^2 \pi b_1^2 \omega_0^2}{2} \sum_{j=1}^J j^2 F(j)^2 [\delta(\omega - \omega_j) + \delta(\omega + \omega_j)]. \end{aligned}$$

Obviously, the total power spectral density reads $S(\omega) = 0$, and the decoherence function also vanishes, i.e., $\chi(t) = 0$.

We calculate the uncertainty of the measurement by the Fisher information as

$$\delta \Omega_0^2 = \frac{1}{(T/t)F(\phi)} = \frac{1 - \cos^2[(N\omega_0 - \omega_a)t]}{N^2 T t \sin^2[(N\omega_0 - \omega_a)t]}. \quad (57)$$

By similar derivation to Eq. (27), we have $\delta \Omega_0^2|_{e\propto} (n-1)^{-2}$. We find the scaling law for our scheme can approach the HL when N is large enough, even in the case of superdecoherence.

We apply the quantum simulation algorithm to simulate our scheme with $N = 100$, $\Omega_0 = 2\pi \times 25$ kHz, $\alpha = 125$ s⁻¹, $\beta = 4.2473 \times 10^4$ s⁻², as shown in Fig. 4. We use the same types of lines as Fig. 2 to represent the probability. Here the number

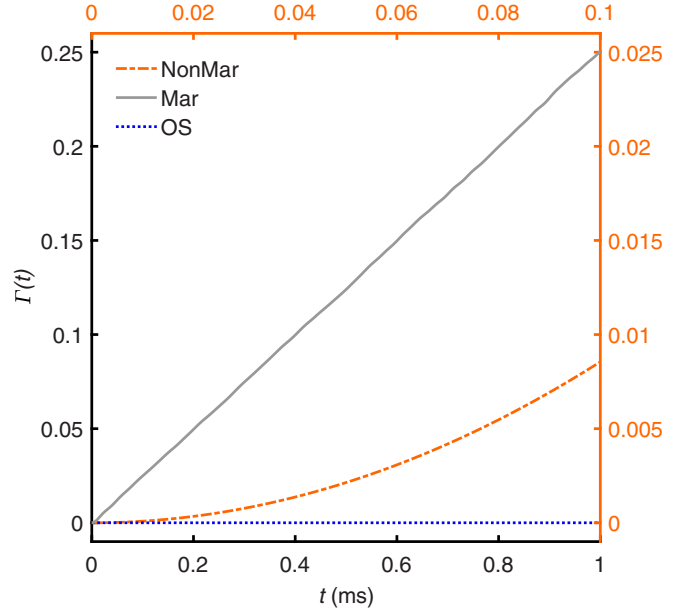


FIG. 5. The simulated decoherence factor $\Gamma(t)$ for different schemes: the gray solid line for the Markovian environment, the red dash-dotted line for the non-Markovian environment, and the blue dotted line for our scheme. Notice that the double axes are used to show the different timescales of the two environments.

of random realizations in ensemble we used in this simulation is 2×10^4 . Without loss of generality, we assume the model of white noise, i.e., $F(j) = 1/j$ [34]. For a ¹³C-labeled trans-crotonic acid which is used as a four-qubit simulator, the shortest T_2 of C nuclear spins is 0.87 second [62]. The parameters are chosen according to the requirement that the longest duration in the metrology is much shorter than the timescale of pure dephasing. Because the transverse relaxation time of the NMR platform is of the order of seconds, we choose suitable parameters to ensure that the simulated dephasing time is much less than the real T_2 . In the uncorrelated Markovian decoherence, the base and cutoff frequencies are respectively $\omega_0 = 2$ kHz and $\omega_c = 2$ MHz, and the noise amplitude is $b_1^2 = 4.109692 \times 10^{-3} \hbar^2$. In the Markovian superdecoherence, the parameters are respectively $\omega_0 = 20$ kHz, $\omega_c = 0.2$ GHz, and $b_1^2 = 4.109692 \times 10^{-3} \hbar^2$. For the non-Markovian noises, we use the following parameters for both cases, i.e., $\omega_0 = 0.001$ Hz, $\omega_c = 0.18$ Hz, and $b_1^2 = 4.7192 \times 10^8 \hbar^2$. We can learn from Fig. 4 that the results of the stochastic Hamiltonian simulation are in quite-good agreement with the results of the Bloch-Redfield equation. The blue square dots represent our scheme, which implies that employing one auxiliary qubit can cancel the effects of noise. As a result, the precision in our scheme can approach the HL. In order to explore the underlying physical mechanism explicitly, we also plot the corresponding decoherence factor $\Gamma(t)$ in Fig. 5. For the Markovian noise, the coherence decays with a constant rate, and thus using entangled probes will not improve the precision of the estimation. For the non-Markovian noise, since the coherence decays quadratically with time, the use of the entangled probe can offer a better estimation, but the precision is still lower than the HL. However, for a correlated bath,

because all qubits suffer from the collective noise, by properly arranging the auxiliary qubit the noises on the working qubits can be effectively canceled and thus the noise-free measurement can be performed.

Superdecoherence has been observed experimentally in the ion-trap system with $^{40}\text{Ca}^+$ ions [52,63]. Therein the noise is mainly caused by fluctuations of the homogeneous magnetic field [52]. In order to demonstrate our scheme, we may insert one additional ion into the trap as the auxiliary particle, which is more sensitive to the magnetic field, e.g., with the gyromagnetic ratio about N times that of the system qubit. For example, the gyromagnetic ratio of $S_{1/2}(m = -1/2) \leftrightarrow D_{5/2}(m = 1/2)$ is four times that of $S_{1/2}(m = -1/2) \leftrightarrow D_{5/2}(m = -1/2)$ [64]. By choosing appropriate qubit states, the scheme with $N = 2, 4, 5, 7$ can be realized, and the additional magnetic field to be measured is only applied to the system qubits. Furthermore, if we initially prepare an $(N + 1)$ -qubit entangled state as in Eq. (18), e.g., $N = 4$, it could be a potential realistic implementation of our scheme.

IV. CONCLUSION

In this paper we propose a quantum metrology scheme with auxiliary states. The auxiliary states are properly designed and can selectively offset the impact of environmental noise. On account of superdecoherence, we analyze the optimal precision with and without auxiliary qubits. We find out that when the auxiliary qubits are not employed, the precision cannot be improved by using the entangled probes no matter whether the noise is Markovian or non-Markovian. However, utilizing an auxiliary qubit can make the precision approach the HL in our scheme. We further discuss the cases of an uncorrelated and partially correlated environment and find that employing auxiliary qubits can improve the precision of measurement in the partially correlated environment, but it fails in the uncorrelated environment. As an example, we show how to utilize our scheme with one auxiliary qubit in magnetic-field sensing. Finally, we use the bath-engineering technique and GRAPE to simulate the quantum dynamics and demonstrate that assisted by an auxiliary qubit, our scheme can approach the HL in the case of superdecoherence.

ACKNOWLEDGMENTS

We are thankful for valuable discussions with J.-H. An and M.-J. Tao. This work is supported by the National Natural

Science Foundation of China under Grants No. 11674033, No. 11474026, and No. 11505007, and the Beijing Natural Science Foundation under Grant No. 1202017.

APPENDIX: GRADIENT ASCENT PULSE ENGINEERING ALGORITHM

The GRAPE algorithm has been widely used in NMR experiments [35,36]. For an n -qubit NMR system, the total Hamiltonian H_{tot} is composed of the internal term H_{int} and the rf term

$$H_{\text{RF}} = - \sum_{k=1}^n \gamma_k B_k [\cos(\omega_k^{\text{RF}} t + \phi_k^{\text{RF}}) \sigma_x^{(k)} + \sin(\omega_k^{\text{RF}} t + \phi_k^{\text{RF}}) \sigma_y^{(k)}], \quad (\text{A1})$$

where γ_k and $\sigma_\alpha^{(k)}$ ($\alpha = x, y, z$) are respectively the gyromagnetic ratio and the Pauli operators of the k th nuclear spin, and B_k , ω_k^{RF} , and ϕ_k^{RF} are the amplitude, driving frequency, and phase of the control field on the k th nuclear spin, respectively.

The aim of the GRAPE algorithm is to find the optimal amplitudes B_k 's and phases ϕ_k^{RF} 's by iteration, so as to make the designed unitary evolution U_D very close to the target evolution U_T . The fidelity of U_D relative to U_T can be expressed as $F = |\text{Tr}(U_T^\dagger U_D)|/2^n$. By dividing the total evolution time T into N steps, the time of each step is $\Delta t = T/N$, and thus the time evolution operator of the j th step can be expressed as

$$U_j = e^{-i\Delta t [H_{\text{int}} + \sum_{k=1}^n \sum_{\alpha=x,y} u_\alpha^{(k)}(j) \sigma_\alpha^{(k)}]}, \quad (\text{A2})$$

where $u_x^{(k)}(j) = \gamma_k B_k \cos(\omega_k^{\text{RF}} t_j + \phi_k^{\text{RF}})$ and $u_y^{(k)}(j) = \gamma_k B_k \sin(\omega_k^{\text{RF}} t_j + \phi_k^{\text{RF}})$. The total evolution operator can be given as $U_D = U_N U_{N-1} \dots U_2 U_1$. The gradient of the fidelity F with respect to $u_\alpha^{(k)}(j)$ is

$$\begin{aligned} g_\alpha^{(k)}(j) &= \frac{\partial F}{\partial u_\alpha^{(k)}(j)} \\ &\approx -\frac{2}{2^n} \text{Re}[U_T^\dagger U_N \dots U_{j+1} (-i\Delta t \sigma_\alpha^{(k)}) U_j \dots U_1]. \end{aligned} \quad (\text{A3})$$

The GRAPE algorithm starts with an initial guess input and is followed by the gradient iteration to increase the fidelity. We replace $u_\alpha^{(k)}(j)$ by $u_\alpha^{(k)}(j) + \epsilon_s g_\alpha^{(k)}(j)$, where ϵ_s is the iteration step, until the fidelity changes less than the selected threshold.

[1] V. Giovannetti, S. Lloyd, and L. Maccone, Advances in quantum metrology, *Nat. Photonics* **5**, 222 (2011).
 [2] C. L. Degen, F. Reinhard, and P. Cappellaro, Quantum sensing, *Rev. Mod. Phys.* **89**, 035002 (2017).
 [3] M. A. Nielsen and I. L. Chuang, *Quantum Computation and Quantum Information* (Cambridge University Press, Cambridge, England, 2000).
 [4] N. Lambert, Y. N. Chen, Y. C. Cheng, C. M. Li, G. Y. Chen, and F. Nori, Quantum biology, *Nat. Phys.* **9**, 10 (2013).
 [5] Q. Ai, T. C. Yen, B. Y. Jin, and Y. C. Cheng, Clustered geometries exploiting quantum coherence effects for efficient

energy transfer in light harvesting, *J. Phys. Chem. Lett.* **4**, 2577 (2013).
 [6] C. Y. Cai, Q. Ai, H. T. Quan, and C. P. Sun, Sensitive chemical compass assisted by quantum criticality, *Phys. Rev. A* **85**, 022315 (2012).
 [7] L. P. Yang, Q. Ai, and C. P. Sun, Generalized Holstein model for spin-dependent electron-transfer reactions, *Phys. Rev. A* **85**, 032707 (2012).
 [8] J. M. Cai and M. B. Plenio, Chemical Compass Model for Avian Magnetoreception as a Quantum Coherent Device, *Phys. Rev. Lett.* **111**, 230503 (2013).

- [9] M. Ö. Oktel and Ö. E. Müstecaplıoğlu, Electromagnetically induced left-handedness in a dense gas of three-level atoms, *Phys. Rev. A* **70**, 053806 (2004).
- [10] Q. Thommen and P. Mandel, Electromagnetically Induced Left Handedness in Optically Excited Four-Level Atomic Media, *Phys. Rev. Lett.* **96**, 053601 (2006).
- [11] J. Kästel, M. Fleischhauer, S. F. Yelin, and R. L. Walsworth, Tunable Negative Refraction without Absorption via Electromagnetically Induced Chirality, *Phys. Rev. Lett.* **99**, 073602 (2007).
- [12] J. X. Zhao, J. J. Cheng, Y. Q. Chu, Y. X. Wang, F. G. Deng, and Q. Ai, Hyperbolic metamaterial using chiral molecules, *Sci. China-Phys. Mech. Astron.* **63**, 260311 (2020).
- [13] S. L. Braunstein, Quantum Limits on Precision Measurements of Phase, *Phys. Rev. Lett.* **69**, 3598 (1992).
- [14] V. Giovannetti, S. Lloyd, and L. Maccone, Quantum-enhanced measurements: Beating the standard quantum limit, *Science* **306**, 5700 (2004).
- [15] D. Leibfried, M. D. Barrett, T. Schaetz, J. Britton, J. Chiaverini, W. M. Itano, J. D. Jost, C. Langer, and D. J. Wineland, Toward Heisenberg-limited spectroscopy with multiparticle entangled states, *Science* **304**, 5676 (2004).
- [16] C. Roos, M. Chwalla, K. Kim, M. Riebe, and R. Blatt, ‘Designer atoms’ for quantum metrology, *Nature (London)* **443**, 316 (2006).
- [17] H.-P. Breuer, E.-M. Laine, J. Piilo, and B. Vacchini, Colloquium: Non-Markovian dynamics in open quantum systems, *Rev. Mod. Phys.* **88**, 021002 (2016).
- [18] I. de Vega and D. Alonso, Dynamics of non-Markovian open quantum systems, *Rev. Mod. Phys.* **89**, 015001 (2017).
- [19] L. Li, M. J. W. Hall, and H. M. Wiseman, Concepts of quantum non-Markovianity: A hierarchy, *Phys. Rep.* **759**, 1 (2018).
- [20] H.-P. Breuer, E.-M. Laine, and J. Piilo, Degree of Non-Markovian Behavior of Quantum Processes in Open Systems, *Phys. Rev. Lett.* **103**, 210401 (2009).
- [21] B.-H. Liu, L. Li, Y.-F. Huang, C.-F. Li, G.-C. Guo, E.-M. Laine, H.-P. Breuer, and J. Piilo, Experimental control of the transition from Markovian to non-Markovian dynamics of open quantum systems, *Nat. Phys.* **7**, 931 (2011).
- [22] A. Rivas, S. F. Huelga, and M. B. Plenio, Entanglement and Non-Markovianity of Quantum Evolutions, *Phys. Rev. Lett.* **105**, 050403 (2010).
- [23] L. Childress, M. V. G. Dutt, J. M. Taylor, A. S. Zibrov, F. Jelezko, J. Wrachtrup, P. R. Hemmer, and M. D. Lukin, Coherent dynamics of coupled electron and nuclear spin qubits in diamond, *Science* **314**, 281 (2006).
- [24] Y. Matsuzaki, S. C. Benjamin, and J. Fitzsimons, Magnetic field sensing beyond the standard quantum limit under the effect of decoherence, *Phys. Rev. A* **84**, 012103 (2011).
- [25] A. W. Chin, S. F. Huelga, and M. B. Plenio, Quantum Metrology in Non-Markovian Environments, *Phys. Rev. Lett.* **109**, 233601 (2012).
- [26] K. Bai, Z. Peng, H.-G. Luo, and J.-H. An, Retrieving Ideal Precision in Noisy Quantum Optical Metrology, *Phys. Rev. Lett.* **123**, 040402 (2019).
- [27] Y.-S. Wang, C. Chen, and J.-H. An, Quantum metrology in local dissipative environments, *New J. Phys.* **19**, 113019 (2017).
- [28] J. Kattemölle and J. van Wezel, Conditions for superdecoherence, *Quantum* **4**, 265 (2020).
- [29] Z. H. Wang, Y. J. Ji, Y. Li, and D. L. Zhou, Dissipation and decoherence induced by collective dephasing in a coupled-qubit system with a common bath, *Phys. Rev. A* **91**, 013838 (2015).
- [30] U. Dörner, Quantum frequency estimation with trapped ions and atoms, *New J. Phys.* **14**, 043011 (2012).
- [31] R. Yousefjani, S. Salimi, and A. S. Khorashad, Enhancement of frequency estimation by spatially correlated environments, *Ann. Phys. (NY)* **381**, 80 (2017).
- [32] X.-K. Song, H. Zhang, Q. Ai, J. Qiu, and F.-G. Deng, Shortcuts to adiabatic holonomic quantum computation in decoherence-free subspace with transitionless quantum driving algorithm, *New J. Phys.* **18**, 023001 (2016).
- [33] A. Soare, H. Ball, D. Hayes, J. Sastrawan, M. C. Jarratt, J. J. McLoughlin, X. Zhen, T. J. Green, and M. J. Biercuk, Experimental noise filtering by quantum control, *Nat. Phys.* **10**, 825 (2014).
- [34] A. Soare, H. Ball, D. Hayes, X. Zhen, M. C. Jarratt, J. Sastrawan, H. Uys, and M. J. Biercuk, Experimental bath engineering for quantitative studies of quantum control, *Phys. Rev. A* **89**, 042329 (2014).
- [35] N. Khaneja, T. Reiss, C. Kehlet, T. Schulte-Herbrüggen, and S. J. Glaser, Optimal control of coupled spin dynamics: Design of NMR pulse sequences by gradient ascent algorithms, *J. Magn. Reson.* **172**, 296 (2005).
- [36] J. Li, X. D. Yang, X. H. Peng, and C. P. Sun, Hybrid Quantum-Classical Approach to Quantum Optimal Control, *Phys. Rev. Lett.* **118**, 150503 (2017).
- [37] B.-X. Wang, M.-J. Tao, Q. Ai, T. Xin, N. Lambert, D. Ruan, Y.-C. Cheng, F. Nori, F.-G. Deng, and G.-L. Long, Efficient quantum simulation of photosynthetic light harvesting, *npj Quantum Inf.* **4**, 52 (2018).
- [38] N.-N. Zhang, M.-J. Tao, W.-T. He, X.-Y. Chen, X.-Y. Kong, F.-G. Deng, N. Lambert, and Q. Ai, Efficient quantum simulation of open quantum dynamics at various Hamiltonians and spectral densities, *Front. Phys.* **16**, 51501 (2021).
- [39] I. Buluta and F. Nori, Quantum simulators, *Science* **326**, 108 (2009).
- [40] I. M. Georgescu, S. Ashhab, and F. Nori, Quantum simulation, *Rev. Mod. Phys.* **86**, 153 (2014).
- [41] A. J. Leggett, S. Chakravarty, A. T. Dorsey, M. P. A. Fisher, A. Garg, and W. Zwerger, Dynamics of the dissipative two-state system, *Rev. Mod. Phys.* **59**, 1 (1987).
- [42] M.-J. Tao, N.-N. Zhang, P.-Y. Wen, F.-G. Deng, Q. Ai, and G.-L. Long, Coherent and incoherent theories for photosynthetic energy transfer, *Sci. Bull.* **65**, 318 (2020).
- [43] J. Jeske and J. H. Cole, Derivation of Markovian master equations for spatially correlated decoherence, *Phys. Rev. A* **87**, 052138 (2013).
- [44] J. Piilo, S. Maniscalco, K. Härkönen, and K.-A. Suominen, Non-Markovian Quantum Jumps, *Phys. Rev. Lett.* **100**, 180402 (2008).
- [45] Q. Ai, Y. J. Fan, B. Y. Jin, and Y. C. Cheng, An efficient quantum jump method for coherent energy transfer dynamics in photosynthetic systems under the influence of laser fields, *New J. Phys.* **16**, 053033 (2014).
- [46] H. P. Breuer and F. Petruccione, *The Theory of Open Quantum Systems* (Oxford University Press, Oxford, England, 2002).
- [47] J. Jeske, D. J. Ing, M. B. Plenio, S. F. Huelga, and J. H. Cole, Bloch-Redfield equations for modeling light-harvesting complexes, *J. Chem. Phys.* **142**, 064104 (2015).

- [48] G. M. Palma, K.-A. Suominen, and A. Ekert, Quantum computers and dissipation, *Proc. R. Soc. London, Ser. A* **452**, 567 (1996).
- [49] S. F. Huelga, C. Macchiavello, T. Pellizzari, A. K. Ekert, M. B. Plenio, and J. I. Cirac, Improvement of Frequency Standards with Quantum Entanglement, *Phys. Rev. Lett.* **79**, 3865 (1997).
- [50] P. Liu, P. Wang, W. Yang, G. R. Jin, and C. P. Sun, Fisher information of a squeezed-state interferometer with a finite photon-number resolution, *Phys. Rev. A* **95**, 023824 (2017).
- [51] J. H. Reina, L. Quiroga, and N. F. Johnson, Decoherence of quantum registers, *Phys. Rev. A* **65**, 032326 (2002).
- [52] T. Monz, P. Schindler, J. T. Barreiro, M. Chwalla, D. Nigg, W. A. Coish, M. Harlander, W. Hänsel, M. Hennrich, and R. Blatt, 14-Qubit Entanglement: Creation and Coherence, *Phys. Rev. Lett.* **106**, 130506 (2011).
- [53] Q. Ai, Y. Li, H. Zheng, and C. P. Sun, Quantum anti-Zeno effect without rotating wave approximation, *Phys. Rev. A* **81**, 042116 (2010).
- [54] Q. Ai, D. Xu, S. Yi, A. G. Kofman, C. P. Sun, and F. Nori, Quantum anti-Zeno effect without wave function reduction, *Sci. Rep.* **3**, 1752 (2013).
- [55] P. M. Harrington, J. T. Monroe, and K. W. Murch, Quantum Zeno Effects from Measurement Controlled Qubit-Bath Interactions, *Phys. Rev. Lett.* **118**, 240401 (2017).
- [56] F. Schmidt-Kaler, H. Häffner, S. Gulde, M. Riebe, G. P. T. Lancaster, T. Deuschle, C. Becher, W. Hänsel, J. Eschner, C. F. Roos, and R. Blatt, How to realize a universal quantum gate with trapped ions, *Appl. Phys. B* **77**, 789 (2003).
- [57] N. Zhao, S.-W. Ho, and R.-B. Liu, Decoherence and dynamical decoupling control of nitrogen vacancy center electron spins in nuclear spin baths, *Phys. Rev. B* **85**, 115303 (2012).
- [58] L.-S. Li, H.-H. Li, L.-L. Zhou, Z.-S. Yang, and Q. Ai, Measurement of weak static magnetic field with nitrogen-vacancy color center, *Acta Phys. Sin.* **66**, 230601 (2017).
- [59] A. Jarmola, V. M. Acosta, K. Jensen, S. Chemerisov, and D. Budker, Temperature- and Magnetic-Field-Dependent Longitudinal Spin Relaxation in Nitrogen-Vacancy Ensembles in Diamond, *Phys. Rev. Lett.* **108**, 197601 (2012).
- [60] Z.-S. Yang, Y.-X. Wang, M.-J. Tao, W. Yang, M. Zhang, Q. Ai, and F.-G. Deng, Longitudinal relaxation of a nitrogen-vacancy center in a spin bath by generalized cluster-correlation expansion method, *Ann. Phys. (NY)* **413**, 168063 (2020).
- [61] K. Head-Marsden, J. Flick, C. J. Ciccarino, and P. Narang, Quantum information and algorithms for correlated quantum matter, *Chem. Rev.* **121**, 3061 (2021).
- [62] T. Xin, J. S. Pedernales, E. Solano, and G.-L. Long, Entanglement measures in embedding quantum simulators with nuclear spins, *Phys. Rev. A* **97**, 022322 (2018).
- [63] L. Pezzè, A. Smerzi, M. K. Oberthaler, R. Schmied, and P. Treutlein, Quantum metrology with nonclassical states of atomic ensembles, *Rev. Mod. Phys.* **90**, 035005 (2018).
- [64] J. Zhang, W. Wu, C. W. Wu, J. G. Miao, Y. Xie, B. Q. Ou, and P. X. Chen, Discrimination and estimation for dephasing sources of trapped ion qubits, *Appl. Phys. B* **126**, 20 (2020).